Acta Astronautica 142 (2018) 121–129

Contents lists available at ScienceDirect

Acta Astronautica

journal homepage: www.elsevier.com/locate/actaastro

Formation mechanisms and characteristics of transition patterns in oblique detonations

Shikun Miao, Jin Zhou *, Shijie Liu, Xiaodong Cai

National University of Defense Technology, 410073 Changsha, People's Republic of China

ARTICLE INFO

Keywords:
Numerical simulation
Oblique detonation wave
Transition structure
Formation mechanisms
Quantitative criterion

ABSTRACT

The transition structures of wedge-induced oblique detonation waves (ODWs) in high-enthalpy supersonic combustible mixtures are studied with two-dimensional reactive Euler simulations based on the open-source program AMROC (Adaptive Mesh Refinement in Object-oriented C++). The formation mechanisms of different transition patterns are investigated through theoretical analysis and numerical simulations. Results show that transition patterns of ODWs depend on the pressure ratio P_d/P_s, (P_d, P_s are the pressure behind the ODW and the pressure behind the induced shock, respectively). When $P_d/P_s > 1.3$, an abrupt transition occurs, while when $P_d/P_s < 1.3$, a smooth transition appears. A parameter ε is introduced to describe the transition patterns quantitatively. Besides, a criterion based on the velocity ratio $\Phi=U_0/U_{CJ}$ is proposed to predict the transition patterns based on the inflow conditions. It is concluded that an abrupt transition appears when $\Phi < 0.98\Phi^*$, while a smooth transition occurs when $\Phi > 1.02\Phi^*$ (Φ^* is the critical velocity ratio calculated with an empirical formula).

1. Introduction

The oblique detonation wave engine (ODWE) concept offers the potential for greater efficiency at higher Mach numbers [1–4] in comparison with the traditional scramjet. In the combustor of an ODWE, the oblique detonation wave (ODW) is initiated and stabilized by a wedge, and combustion occurs near the detonation wave front, which enables structure simplification and loss minimization of the engine. However, due to the complexity of ODW structure and the difficulty in performing experimental studies, there remain lots of challenges in the development of ODWE. It is still of great interest to conduct research on the basic structure of ODWs.

The ODWs are always classified based on the transition structure, i.e. smooth transition and abrupt transition, which are shown in Fig. 1.

In early studies, the ODW was usually simplified into a strong oblique shock with an instantaneous post-shock heat release. Until 1990s, Li et al. [5,6] investigated the structure of ODW and mentioned that the ODW structure consists of a non-reactive oblique shock, an induction zone, a set of deflagration waves and an oblique detonation wave. The transition from the non-reactive shock to the oblique detonation wave is achieved abruptly, and they are separated by a triple-point. Later, Broda [7] conducted experimental studies on ODWs and observed a smooth transition from oblique shock to oblique detonation. Vlasenko et al. [8] performed a numerical study on the wedge-induced ODW with an algorithm they developed and a smooth transition was also observed in their results. Viguier et al. [9] studied the structure of stable oblique detonations both numerically and experimentally. Their simulation results showed a good agreement with the overall flow structure observed experimentally, which is also consistent with that in Refs. [5,6]. Gui et al. [10] investigated the ODW with a Mach 7 inflow over a wedge of 30° turning angle numerically. According to their results, the ODW front is composed of oblique shock wave and oblique detonation when the wedge length is short. However, when the wedge is long enough, the flow field behind ODW is divided into three regions: ZND-model-like structure; single-sided, triple-point structure; and dual-headed, triple-point structure. Liu et al. [11] investigated the wedge-induced ODWs at low inflow Mach numbers via Rankine-Hugoniot analysis and numerical simulations. Their results showed that the strengthening influence of Chapman-Jouguet (CJ) detonation wave can lead to an upstream propagation of the ODW, and during this process, a Mach reflection wave configuration is always established on the wedge. Lately, Liu et al. [12] have made some further investigations on the structures of wedge-induced ODWs via the same method as Ref. [11]. In their numerical results, four configurations of CJ ODW reflection (overall Mach reflection, Mach reflection, regular reflection, and non-reflection) are observed to take place sequentially as the inflow Mach number increases,

* Corresponding author.
E-mail address: zj706@vip.sina.com (J. Zhou).

https://doi.org/10.1016/j.actaastro.2017.10.035
Received 23 May 2017; Received in revised form 26 September 2017; Accepted 28 October 2017
Available online 5 November 2017

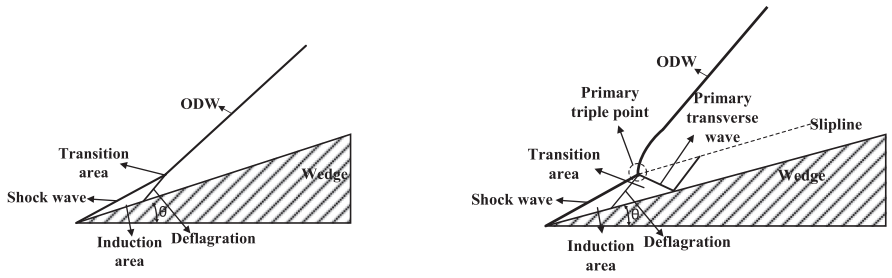

(a) Smooth transition (b) Abrupt transition

Fig. 1. Schematic diagram of ODWs with different transition structures.

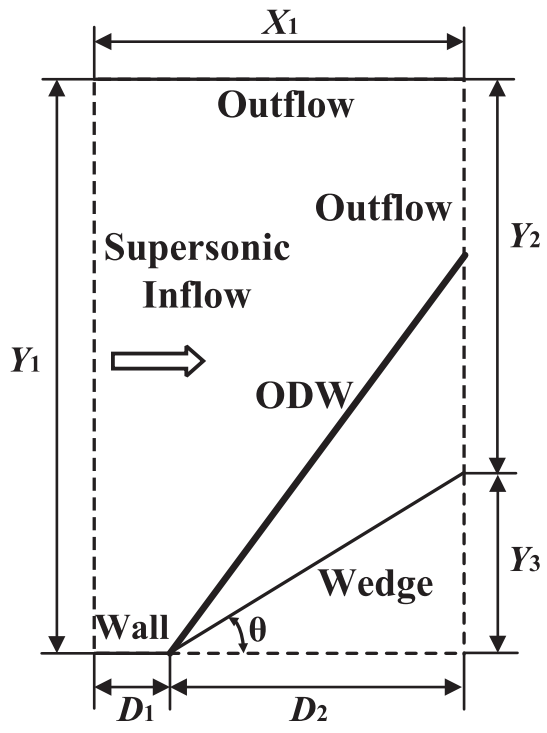

Fig. 2. The schematic of the calculation model.

and the change of the configuration results from the interaction among the ODW, the CJ ODW, and the centered expansion wave.

Recently, studies on transition patterns of ODWs have been specially conducted. Lefebvre and Fujiwara [13] simulated ODWs with different inflow Mach numbers and the effects of blunt body size on detonation structures were investigated. They argued that a smooth transition appears when the blunt body is large, while an abrupt transition forms under a small size of blunt body. Papalexandris et al. [14] observed the transition structures at different wedge angles, and the results showed that for moderate wedge angles the induced shock curves smoothly and for higher wedge angles an explosion occurs at the induced shock, leading to an abrupt transition. Teng et al. [15] studied the induction zone structures with different incident Mach numbers and three kinds of shock configurations, i.e., the λ-shaped shock, X-shaped shock and Y-shaped shock, were observed at the end of the induction zone. In the most recent research of Teng et al. [16], the initiation features of a wedge-induced ODW were investigated via numerical simulations. The effects of inflow pressure and Mach number on the initiation structure and length were studied. And the results demonstrated that the transition patterns strongly depend on the inflow Mach number, while the inflow pressure is found to have little effects on the transition type. Furthermore, a few quantitative investigations on the transition patterns have been conducted. Silva and Dashaies [17] may be the first to explore the criterion to predict the transition structures of ODWs. In their study, ODWs with different wedge angles, temperatures and pressures were investigated and the time ratio t_i/t_r was proposed for the estimation of transition patterns, where t_i and t_r are the induction time and the total reaction time, respectively. When $t_i/t_r \to 0$, the transition is abrupt and when $t_i/t_r \to 1$, it is smooth. However, the time ratio is a zero-dimensional scalar, it may not be convincing enough to describe a two-dimensional or three-dimensional phenomenon, and the wedge angle was not included in this criterion. Afterwards, Wang et al. [18] examined the existence or inexistence of the primary transverse wave in wedge-induced ODWs. A criterion associated with the ratio $\varphi = U_2/U_{CJ}$ was chosen to estimate the transition structures, where U_2 is the flow velocity behind the ODW and U_{CJ} is the CJ speed of the ODW. They indicated that when $\varphi < 1$, an abrupt transition occurs, and when $\varphi > 1$, a smooth transition forms. However, the formation mechanisms of different transition patterns were not explained in their paper and the ratio is not so convenient when applied to the prediction of transition patterns. Teng et al. [19] studied the transition structures numerically and a criterion based on the difference in the oblique shock angle and detonation angle was raised to predict the transition patterns. They suggested that a smooth transition appears when the angle difference is small, while an abrupt transition occurs when the angle difference is large. The shift between the two different transition patterns occurs when the angle difference is about $15^\circ - 18^\circ$. This criterion is considered to be more applicative for different cases. However, the formation mechanisms of different transition patterns are still not explained clearly.

In the present study, structures of the wedge-induced ODWs are systematically studied based on AMROC [20], which has been validated in multi-dimensional detonation simulations [21–23]. First, the numerical method is introduced and validated in Sections 2 and 3. And then, theoretical analysis and numerical simulations are conducted in Section 4.2 to explain the formation mechanisms of different transition patterns. In Section 4.3, a quantitative criterion is established to predict the transition patterns based on the inflow conditions.

2. Mathematical model and numerical method

2.1. Computational setup

The two-dimensional numerical simulations are conducted in a channel with a fixed wedge, as depicted in Fig. 2. The length and the height of the channel are $X_1 = 70$ mm and $Y_1 = 110$ mm, respectively. The wedge starts from $D_1 = 5$ mm.

The left boundary models the supersonic inflow, while the upper and right boundaries model the outflow. Reflecting boundaries with slip wall conditions are used on the lower boundary and the wedge. To mimic a realistic working condition, high-enthalpy supersonic combustible mixtures are selected. The premixed mixtures consist of hydrogen, oxygen and nitrogen with a mole ratio of $2 \times ER/1/3.76$, where ER is the equivalence ratio. To make a comparison and validation, a representative

Case 1	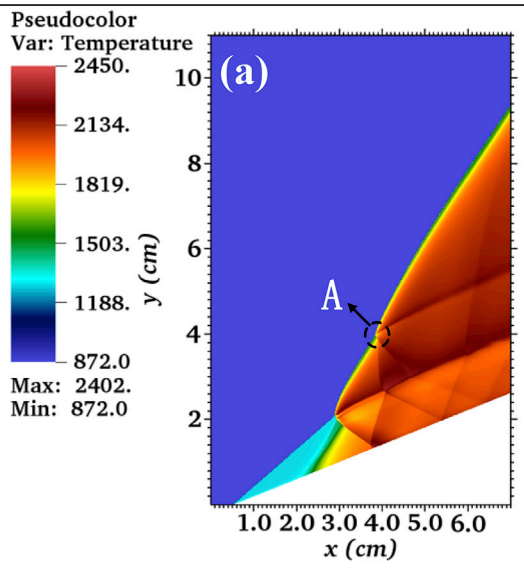	3 levels (2,2) Initial resolution: 0.2 mm t=334 μs Δx_{min}=0.05 mm Grid resolution:20 pts/hrl
Case 2	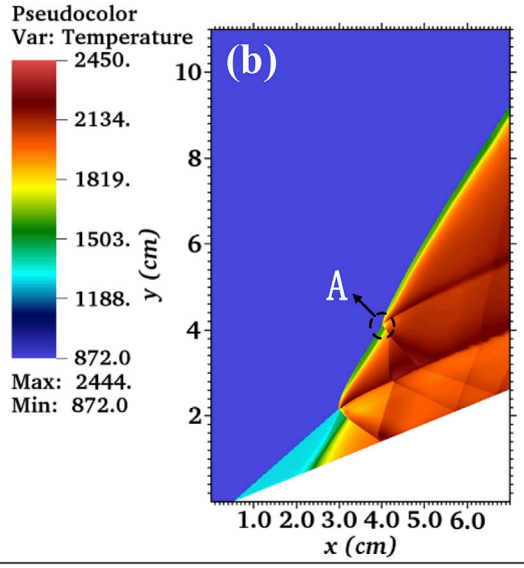	4 levels (2,2,2) Initial resolution: 0.2 mm t=334 μs Δx_{min}=0.025 mm Grid resolution: 40 pts/hrl
Case 3	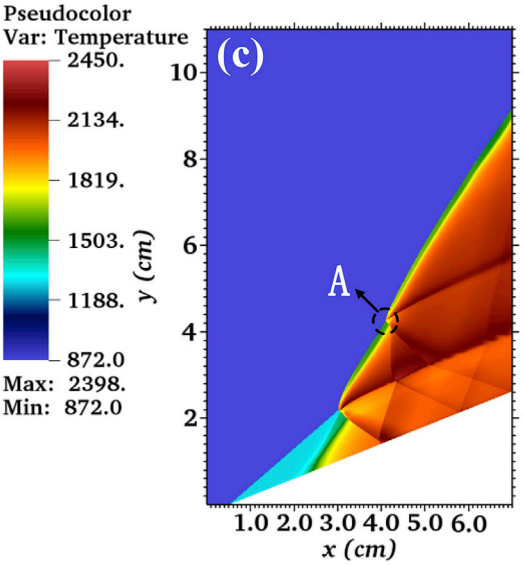	5 levels (2,2,2,2) Initial resolution: 0.2 mm t=334 μs Δx_{min}=0.0125 mm Grid resolution: 80 pts/hrl

Fig. 3. Flow fields with different refinement strategies, $ER = 0.25$, $U_0 = 1690$ m/s, $\theta = 22^{\circ}$.

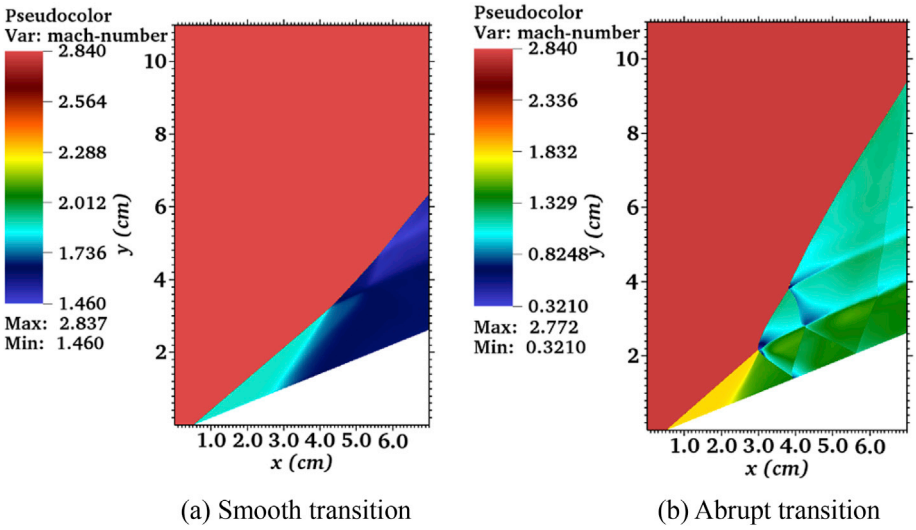

Fig. 4. Mach number pseudocolors of ODWs with different transition patterns, (a) $ER = 0.125$; (b) $ER = 0.25$. (For interpretation of the references to colour in this figure legend, the reader is referred to the web version of this article.)

inflow condition in Ref. [24], i.e. $T_0 = 872$ K, $P_0 = 63$ kPa, is chosen. Actually, the inlet temperature and pressure are found to have little effects on the transition type [16,25], so they are kept unchanged in the present study. The numerical simulations are carried out with different inflow velocities, equivalence ratios and wedge angles. At the beginning of calculation, the channel is filled with a supersonic premixed mixture. A shock-induced combustion occurs with the presence of the wedge and later initiates the ODW.

2.2. Governing equations

Previous numerical studies [17,26] demonstrate that viscosity and boundary layer have little effects on the oblique detonation structure other than changing the boundary layer thickness slightly, and most of previous studies [16,18,19,27] are carried out based on the inviscid assumption. Similarly, the two-dimensional multi-species Euler equations are applied in the present study. A detailed reaction model with 9 species and 19 steps [28] is utilized.

The governing equations are as follows:

$$\frac{\partial \mathbf{U}}{\partial t} + \frac{\partial \mathbf{F}}{\partial x} + \frac{\partial \mathbf{H}}{\partial y} = \mathbf{S} \tag{1}$$

$$\mathbf{U} = (\rho, \rho u, \rho v, \rho e_t, \rho_1, \cdots, \rho_{K-1})^T \tag{2}$$

$$\mathbf{S} = (0, 0, 0, 0, \dot{w}_1, \cdots, \dot{w}_{K-1})^T \tag{3}$$

$$\mathbf{F} = \begin{pmatrix} \rho u \\ \rho u^2 + p \\ \rho uv \\ (\rho e_t + p)u \\ \rho_1 Y_1 u \\ \vdots \\ \rho_{K-1} Y_{K-1} u \end{pmatrix} \quad \mathbf{H} = \begin{pmatrix} \rho v \\ \rho uv \\ \rho v^2 + p \\ (\rho e_t + p)v \\ \rho_1 Y_1 v \\ \vdots \\ \rho_{K-1} Y_{K-1} v \end{pmatrix} \tag{4}$$

where $\mathbf{S}$ is the mass production rate, dictated by the chemical reaction model. K is the number of species, and u, v are the velocity vector components in the direction x and y, respectively. The total density and energy are calculated by:

$$\rho = \sum_{i=1}^{K} \rho_i, \quad e = h - \frac{p}{\rho} + \frac{1}{2}(u^2 + v^2) \tag{5}$$

The pressure of the mixture is calculated by the equation of state $p = \sum_{i=1}^{K} \rho_i \frac{R_0}{W_i} T$, where W_i is the molecular weight and T is the gas temperature.

The specific enthalpy of each specie is calculated by:

$$h_i(T) = h_i^f + \int_{T_f}^{T} c_{pi}(s)ds \tag{6}$$

where h_i^f is the formation enthalpy. The specific heat at constant pressure is calculated with a fitting function based on the temperature, expressed as:

$$c_{pi}(T) = \frac{R_0}{W_i}\left(a_{1i} + a_{2i}T + a_{3i}T^2 + a_{4i}T^3 + a_{5i}T^4\right) \quad i = 1, \ldots, K \tag{7}$$

The parameters in Equation (7) are referred to Ref. [29].

The total enthalpy can be written as $h(T) = \sum_{i=1}^{K} Y_i h_i(T)$. Substituting this equation and $E = e + (u^2 + v^2)/2$ into thermodynamic equation $\rho h - p - \rho e = 0$, we can get the equation:

$$\sum_{i=1}^{K} \rho_i h_i(T) - R_0 T \sum_{i=1}^{K} \frac{\rho_i}{W_i} - \rho E + \rho \frac{u^2 + v^2}{2} = 0 \tag{8}$$

The temperature can be solved from the conserved variables, and then the pressure is calculated through the equation of state.

2.3. Numerical scheme

In the present study, the first-order Godunov splitting method [20,30] is applied for source term decoupling. A second-order MUSCL-TVD finite volume method [20] is adopted for convection flux discretization. The calculation process in AMROC is divided into two steps: numerical flux calculation and reconstruction. In the first step, the inter-cell average fluxes are calculated with an upwind method. Here, a hybrid Roe-HLL Riemann solver is used to avoid nonphysical solutions. In the second step, the Van Albada limiter with MUSCL reconstruction is applied to construct the second-order method in space. The MUSCL-Hancock technique [31] is used for second-order accurate time integration. The dynamically adaptive time step with a target CFL number of 0.9 is used.

3. Validation of numerical method

To establish an appropriate calculation domain, as well as a refinement strategy and mesh adaptation flag parameters, validation of

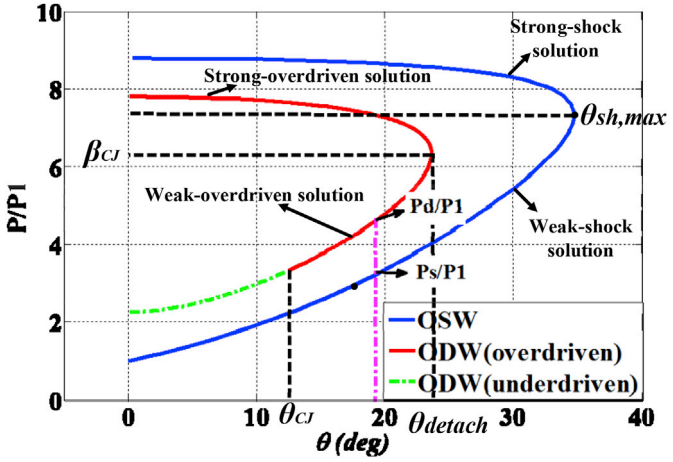

Fig. 5. The shock and detonation polars, $ER = 0.25$, $U_0 = 1690$ m/s.

numerical method is carried out in this section. In the validating case, the inflow velocity is $U_0 = 1690$ m/s, the equivalence ratio is $ER = 0.25$ and the wedge angle is $\theta = 22^{\circ}$. The threshold values for density, temperature, and pressure are $\varepsilon_d = 0.02$, $\varepsilon_T = 100$, and $\varepsilon_p = 4 \times 10^4$ (ε is the scaled gradient), respectively. The initial mesh resolution is 0.2 mm and the refinement levels are 3, 4 and 5, respectively. The highest grid resolutions in the reaction zone are 20 pts/hrl, 40pts/hrl and 80 pts/hrl (pts/hrl is the number of points per half-reaction length), respectively. Fig. 3 shows the flow fields with different refinement strategies.

As shown in Fig. 3, the overall structures of the three flow fields are almost the same, and the primary wave structures are all captured, which is qualitatively consistent with previous studies [18,24]. Thus the adaptation flag parameters are reasonable. However, when observed in detail, two differences are observed at $\Delta x_{\min} = 0.05$ mm (a) The vortex structures along with the slip line are not well observed at $\Delta x_{\min} = 0.05$ mm in comparison with the other two. (b) The induction zone length of case 1 is about 1 mm, as shown in Fig. 3(a). While that of the other two are both 2 mm, as shown in Fig. 3(b) and (c). Actually, the theoretical value calculated with Cantera [32] is 1.984 mm, so the latter two refinement strategies are more accurate. Finally, to balance the calculation resolution and cost, the 4-level refinement strategy is selected for all the following numerical simulations.

4. Result and analysis

4.1. Characteristics of transition patterns

Based on the fixed temperature and pressure, i.e., $T_0 = 872$ K, $P_0 = 63$ kPa, the equivalence ratio, inflow velocity and wedge angle are systematically modified, and ODWs with different transition patterns are achieved under different inflow conditions. The Mach number pseudo-colors of different transition patterns are shown in Fig. 4.

In the case of $ER = 0.125$ (Fig. 4a), an ODW with a smooth transition forms, where the induced shock curves smoothly and transits to oblique detonation without any triple points or transverse waves. Mach numbers behind the ODW decrease a lot, but are still supersonic. In the case of $ER = 0.25$ (Fig. 4b), an ODW with an abrupt transition occurs. The induced shock transits to oblique detonation abruptly, connected by a triple point named primary triple point. The transverse wave originating from the primary triple point is called primary transverse wave, which reflects on the wedge surface. Then the reflected shock wave passes across the slip line and interacts with oblique detonation front, generating the second triple point and resulting in a sharp decrease in Mach number behind the ODW. Especially, flow fields next to triple points and

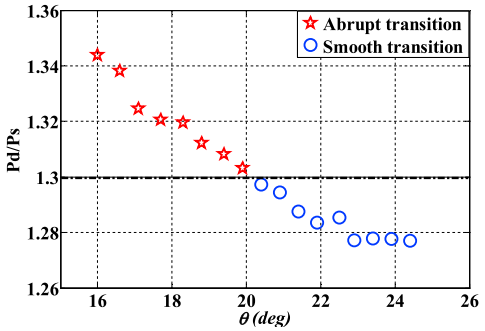

(a) Pressure ratios and transition patterns with different wedge angles, U_0=1870 m/s, ER=0.25

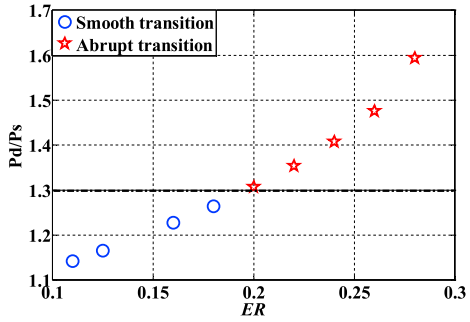

(b) Pressure ratios and transition patterns with equivalence ratios, U_0=1690 m/s, $\theta = 22^{\circ}$

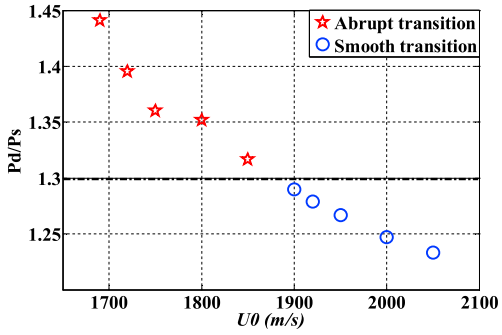

(c) Pressure ratios and transition patterns with different inflow velocities, ER=0.25, $\theta = 22^{\circ}$

Fig. 6. Pressure ratios and transition patterns from numerical simulation results.

transverse waves become subsonic.

4.2. Formation mechanisms of different transition patterns

Although a lot of studies on transition structures have been conducted, the formation mechanisms of different transition patterns are not interpreted clearly. Actually, the existence or inexistence of the primary transverse wave indicates different transition patterns and a shock wave always derives from state difference.

When a shock wave problem in one-dimensional steady flow is considered, the shock wave velocity can be calculated with Eq. (9).

$$V_S = \sqrt{\frac{P_2 - P_1}{\rho_1} \Big/ \frac{\rho_2 - \rho_1}{\rho_2}} = \sqrt{\frac{P_1}{\rho_1}\left(\frac{P_2}{P_1} - 1\right) \Big/ \left(1 - \frac{\rho_1}{\rho_2}\right)} \tag{9}$$

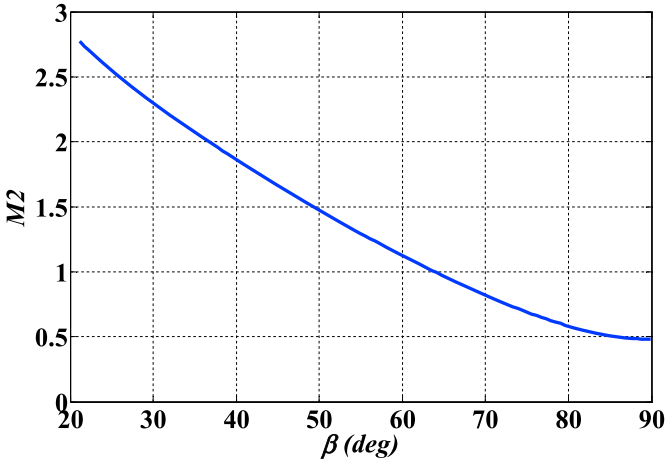

Fig. 7. Post-detonation Mach numbers versus wave angles, $M_1 = 3$, $\gamma = 1.35$.

where V_S is the shock wave velocity. P_1, ρ_1 are the pressure and density ahead of the shock wave, and P_2, ρ_2 are the pressure and density behind the shock wave, respectively. When $P_2/P_1 \to 1$ and $\rho_2/\rho_1 \to 1$, the shock weakens and turns out to be a series of weak compressional waves, and the formula can be written as,

$$V_S = \sqrt{\frac{P_2 - P_1}{\rho_2 - \rho_1}} = \sqrt{\frac{dP}{d\rho}} = c \tag{10}$$

where c is the sound speed.

Therefore, the strength of a shock depends on the pressure ratio P_2/P_1. In the present study, hypotheses are made as follows: (1) the induction zone is followed by a deflagration wave [5,6]; (2) in a certain area close to the primary transverse wave, the flow parameters only change in the direction normal to the transverse wave; (3) the combustible gases are premixed uniformly and moving stably; (4) the flow is considered inviscid and adiabatic. Then the existence of primary transverse wave and the formation mechanisms of different transition patterns can be explained by the pressure ratio P_d/P_s, where P_d is the pressure behind the detonation wave, and P_s is the pressure behind the induced shock. When the pressure ratio is large, the primary transverse wave forms, leading to an abrupt transition. When the pressure ratio is small, the primary transverse wave weakens and fades away, resulting in a smooth transition. To calculate the value of pressure ratio, shock and detonation polars are calculated which are shown in Fig. 5.

It is shown that P_d is always larger than P_s under the same wedge angle θ ($\theta_{CJ} < \theta < \theta_{detach}$, where θ_{CJ} and θ_{detach} are the CJ angle and detachment angle of an ODW, respectively). The pressure ratio P_d/P_s can be calculated by $\frac{P_d}{P_s} = \frac{P_d}{P_0}/\frac{P_s}{P_0}$.

Furthermore, numerical simulations are carried out and different transition patterns are observed. Fig. 6 shows the pressure ratios and transition patterns under different conditions.

It is indicated that, as the wedge angle, equivalence ratio or inflow velocity changes, the transition pattern changes as well, and the position where the transition pattern changes is nearly the same, i.e., $P_d/P_s \cong 1.3$. That means, when $P_d/P_s > 1.3$, an abrupt transition occurs. When $P_d/P_s < 1.3$, a smooth transition appears. Considering the existence of the deflagration wave, the pressure ahead of the primary transverse wave is higher than P_s. So the pressure ratio is actually smaller than 1.3 and is close to 1, which is consistent with the theoretical analysis.

4.3. Parametric analysis of transition patterns

4.3.1. Definition of abrupt degree and smooth degree

Previous investigations on transition structures have always been based on a qualitative description, i.e. abrupt transition and smooth transition. Although some significant conclusions have been achieved, it is not sufficient to conduct intensive quantitative studies. In fact, even the transitions of the same type may differ a lot in stability and wave structure. Therefore, a parameter is needed to quantitatively describe the transition patterns.

Han [24] suggested that the subsonic area behind the ODW is necessary for the formation of primary transverse wave. It was treated as the qualitative criterion to judge the transition pattern. With the existence of the subsonic area, an abrupt transition appears. Otherwise, a smooth transition occurs. In other words, the minimum Mach number behind an ODW indicates the transition pattern. When the minimum is less than 1, subsonic area exists and the transition is abrupt. When the minimum is larger than 1, all the flow fields behind the ODW are supersonic and the transition is smooth.

According to ZND model, the post-detonation Mach number can be calculated by the formula of shock wave,

$$M_2 = \left(\frac{M_1^2 + \frac{2}{\gamma-1}}{\frac{2\gamma}{\gamma-1}M_1^2 \sin^2\beta - 1} + \frac{\frac{2}{\gamma-1}M_1^2 \cos^2\beta}{M_1^2 \sin^2\beta + \frac{2}{\gamma-1}} \right)^{\frac{1}{2}} \tag{11}$$

where M_1 is the inflow Mach number, γ is the specific heat ratio, and β is the angle of ODW. From this formula, the post-shock Mach numbers versus the wave angles are shown in Fig. 7.

It is indicated that the post-detonation Mach number decreases as the wave angle increases. That means, a smaller post-detonation Mach number indicates a larger wave angle, as well as a larger abrupt degree. That means, the minimum Mach number behind the ODW not only indicates different transition patterns but also measures the abrupt degree or smooth degree. Therefore, it is chosen to describe the transition patterns quantitatively.

In the present study, the minimum Mach numbers are obtained from the simulation results, which are always located next to the primary

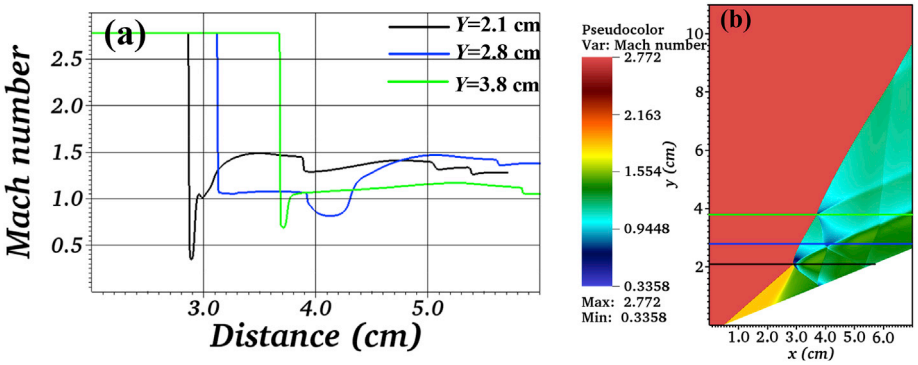

Fig. 8. Mach numbers along with $Y = 2.1$ cm, $Y = 2.8$ cm, and $Y = 3.8$ cm, $ER = 0.25$, $U_0 = 1690$ m/s, $\theta = 22°$.

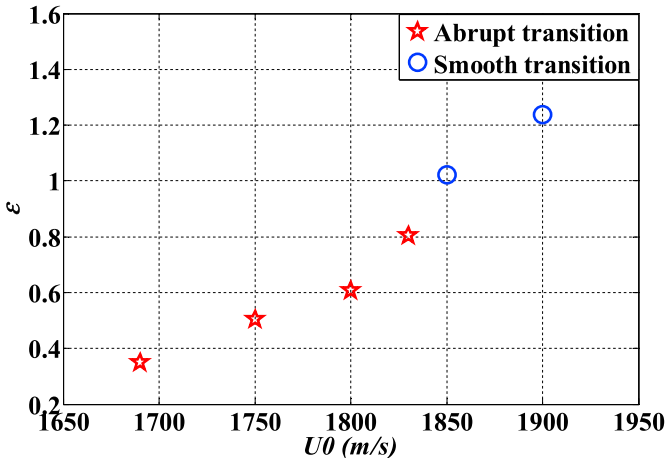

Fig. 9. Values of ε and transition patterns with different inflow velocities, $ER = 0.25$, $\theta = 23^{\circ}$.

triple points. Fig. 8 gives the Mach number along with $Y = 2.1$ cm, $Y = 2.8$ cm and $Y = 3.8$ cm, which demonstrates the location of the minimum Mach number.

It is shown that the minimum Mach number of the whole post-detonation area lies next to the primary triple point. Actually, because of the non-stationarity of the detonation flow field, the minimum post-detonation Mach number always undulates slightly even when the ODW is stable. So an average value is calculated here. After the ODW is stabilized, 10 different moments are selected from a period of 0.1 ms and 10 minimum Mach numbers are obtained. A parameter ε is defined as following,

$$\varepsilon = \overline{M_{2\min}} = \frac{1}{10}\sum_{i=1}^{10}(M_{2\min})_i \tag{12}$$

where $M_{2\min}$ is the minimum Mach number behind the ODW at a moment. When $0 < \varepsilon < 1$, the transition is abrupt and ε is named the abrupt degree. When $\varepsilon > 1$, the transition is smooth and ε is named the smooth degree. With the increase of ε, the transition becomes smoother. Fig. 9 gives the simulation results at $ER = 0.25$ and $\theta = 23^{\circ}$.

It is shown that ε is positive correlated with the inflow velocity and is strictly monotonic, which verifies the rationality of ε.

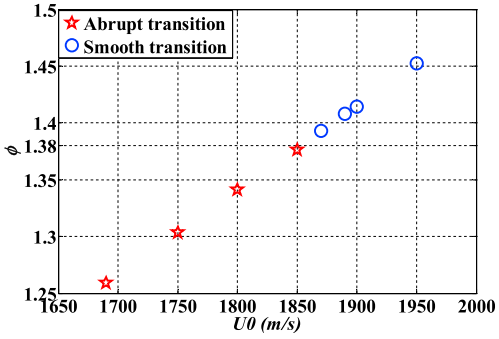

(a) Velocity ratios and transition patterns with different inflow velocities,

ER=0.25, $\theta = 22^{\circ}$

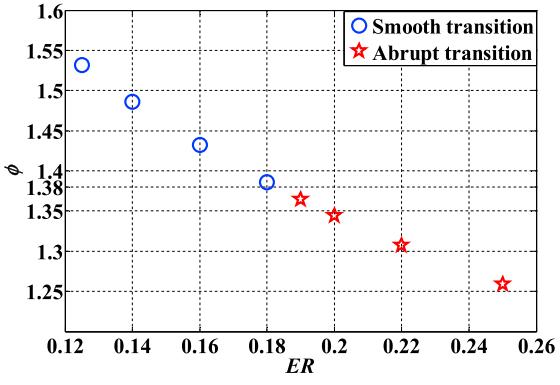

(b) Velocity ratios and transition patterns with different equivalence ratios,

U_0=1690 m/s, $\theta = 22^{\circ}$

Fig. 10. Velocity ratios and transition patterns under different conditions.

4.3.2. Quantitative prediction of the transition pattern

Actually, the propagation of normal detonation waves in the supersonic flow is decided by the inflow velocity U_0 and the CJ speed U_{CJ}. When $U_{CJ} > U_0$, the detonation wave propagates upstream. And when $U_{CJ} < U_0$, the detonation wave propagates downstream. However, for a wedge-induced ODW, when U_{CJ} is greatly smaller than U_0, the ODW front descends instead of propagating downstream and the transition becomes smoother. Therefore, the transition pattern is closely related to U_0 and U_{CJ}, and a quantitative criterion based on the velocity ratio $\Phi = U_0/U_{CJ}$ can be used to predict the transition pattern. In the present study, the CJ speed is calculated with Cantera [32], and the same reaction model as numerical simulations is applied. Fig. 10 shows the velocity ratios and the transition patterns under different conditions.

It is shown that, no matter which factor is changed, the transition pattern changes at the same position, i.e., $\Phi \cong 1.38$. To keep a correspondence with subsequent studies, cases under the influence of inflow velocity are selected, as shown in Table 1.

It is suggested that Φ is positively correlated with ε, which is also monotonic. According to the definition of ε, the transition pattern changes when $\varepsilon = 1$, and there is a critical velocity ratio Φ^*, correspondingly. Apparently, it is nearly impossible to guarantee $\varepsilon = 1$ accurately in the numerical simulations or experimental investigations, so first-order linear interpolation is applied to calculate Φ^*. When $|\varepsilon_1 - \varepsilon_2| < 0.2$ (ε_1, ε_2 is the abrupt degree or smooth degree under different conditions, and $(\varepsilon_1 - 1)(\varepsilon_2 - 1) < 0$), both of ε_1 and ε_2 are considered close enough to 1, and Φ^* is obtained by linear interpolation at the position of $\varepsilon = 1$. In this method, $\Phi^* = 1.3796$ is calculated from Table 1. In other words, for the fixed wedge angle $\theta = 22^{\circ}$, when $\Phi < 1.3796$, an abrupt transition appears and when $\Phi > 1.3796$, a smooth transition pattern occurs.

Obviously, $\Phi^* = 1.3796$ is effective for the wedge angle of $\theta = 22^{\circ}$, and there is a different critical value for a different wedge angle. More numerical simulations are carried out under different wedge angles and the critical velocity ratios are shown in Fig. 11.

It is indicated that the critical velocity ratios are not monotonically related to wedge angles, and a minimum occurs at the position of $\theta \cong 24^{\circ}$. That means, when the inflow velocity increases, a smooth transition is more easily to be formed at this position. Actually, for a given mixture, when the wedge angle is small, the compression effects of the inflow on the wedge surface is relatively weak. Thus the pressure behind the induced shock P_s is lower, and the pressure ratio P_d/P_s is larger. Then a higher inflow velocity is needed for the formation of a smooth transition. On the other hand, when the wedge angle is large, it is close to the detachment angle of the ODW. Under this condition, the ODW is likely to lift and even propagates upstream. And thus, a higher inflow velocity is also required to get a small wave angle for a smooth transition. Therefore, a wedge angle near 24° is more easily to form a smooth transition in a given supersonic combustible mixture.

Table 1
Velocity ratios and transition patterns with different inflow velocities.

U_0 (m/s)	1690	1750	1800	1850	1870	1890	1900	1950
Φ	1.259	1.3036	1.3409	1.376	1.393	1.4079	1.4152	1.4526
ε	0.338	0.4956	0.4854	0.939	1.094	1.1826	1.218	1.37
Transition structure	A	A	A	A	S	S	S	S

A: Abrupt transition, S: Smooth transition.

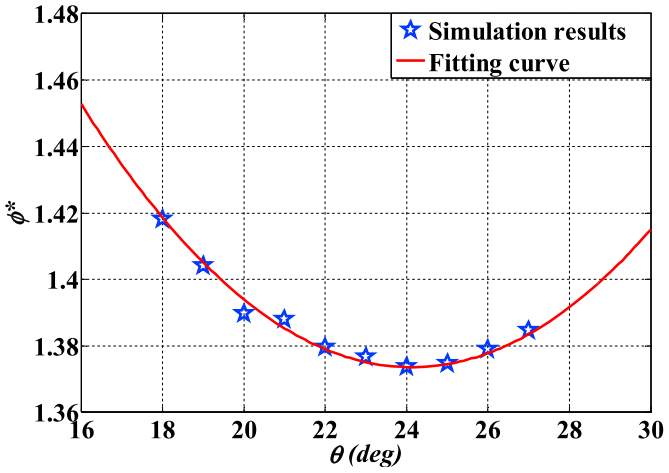

Fig. 11. Critical velocity ratios under different wedge angles.

Based on the simulation results, least square fitting is utilized and an empirical formula between Φ^* and θ is summarized as below,

$$\Phi^* = 0.0012\theta^2 - 0.0579\theta + 2.072 \quad (13)$$

As a comparison, the fitting curve is also shown in Fig. 11.

When the critical velocity ratio Φ^* is obtained, it is possible to predict the transition patterns. That is, an abrupt transition occurs when $\Phi < \Phi^*$, while a smooth transition appears when $\Phi > \Phi^*$. To validate the criterion, two cases with different inflow velocities, i.e., U_{01} = 1920 m/s and U_{02} = 1935 m/s, are selected. The corresponding wedge angle is $\theta = 17^\circ$ and U_{CJ} = 1342.4 m/s. According to the formula, the critical velocity ratio is $\Phi^* = 1.4345$. The velocity ratio for the two cases are $\Phi_1 = 1.4302$ and $\Phi_2 = 1.4414$, respectively. So $\Phi_1 < \Phi^*$ and $\Phi_2 > \Phi^*$. That means the transition is abrupt when U_{01} = 1920 m/s, while it is smooth when U_{02} = 1935 m/s. Numerical simulations are also conducted and the Mach number pseudocolors of the flow fields are shown in Fig. 12.

According to the simulation result, the abrupt degree for Fig. 12(a) is $\varepsilon_1 = 0.9020 < 1$ while the smooth degree for Fig. 12(b) is $\varepsilon_2 = 1.080 > 1$. Therefore, the transition in case 1 is abrupt while that in case 2 is smooth, which is consistent with the prediction through the empirical formula.

To get a further validation, the simulation results of Ref. [18] are listed in Table 2, where the wedge angle is $\theta = 30^\circ$.

According to the empirical formula, $\Phi^* = 1.415$. The velocity ratios for the 3 cases are 1.3294, 1.4184 and 1.5070, respectively. When $M = 7.5$, $\Phi < \Phi^*$, an abrupt transition pattern is supposed to occur, and when $M = 8.0$ or $M = 8.5$, $\Phi > \Phi^*$,a smooth transition is supposed to appear. It is consistent with the results in Table 2, which verifies the usability of the criterion.

However, the velocity ratios of $\Phi_1 = 1.4302$ and $\Phi_2 = 1.4414$ are both very close to the critical value $\Phi^* = 1.4345$, and the structure of the flowfields are very similar as shown in Fig. 12. In fact, when $\phi \cong \phi^*$, the primary transverses wave are so weak that we can hardly distinguish them, and whether the transition patterns are abrupt or smooth is not the key point. In this case, there is no need to make a clear distinction between abrupt transition and smooth transition. Therefore, a limit error of 2% is introduced to avoid this ambiguous critical situation. In other words, an abrupt transition appears when $\Phi < 0.98\phi^*$, and a smooth transition appears when $\Phi > 1.02\phi^*$.

5. Conclusions

In the present study, theoretical analysis and two-dimensional simulations are carried out to investigate the formation mechanisms and characteristics of different transition patterns in ODWs. Theoretical analysis shows that the formation of different transition patterns depends on the pressure ratio P_d/P_s. When $P_d/P_s > 1.3$, the primary transverse wave is formed, and the transition is abrupt. When $P_d/P_s < 1.3$, only weak compressional waves are generated, and the transition is smooth.

Table 2
Verifying results from Ref. [18].

M	U_0	Φ	Transition pattern
7.5	2602.5	1.3298	Abrupt
8.0	2776	1.4184	Smooth
8.5	1949.5	1.5070	Smooth

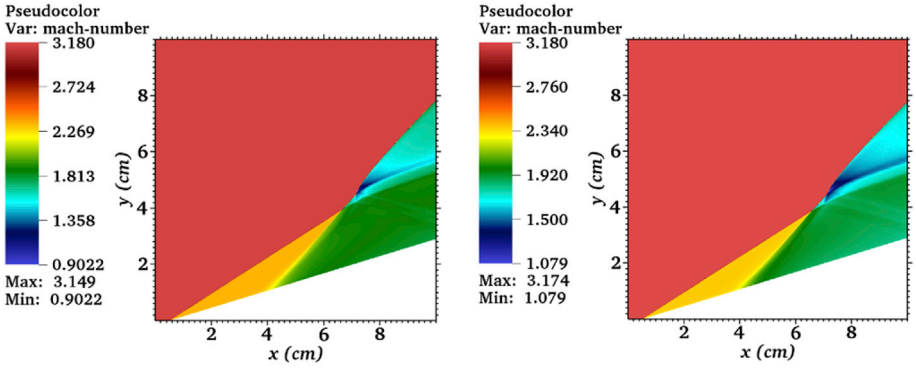

(a) U_{01}=1920 m/s (b) U_{02}=1935 m/s

Fig. 12. Flow fields with different inflow velocities, ER = 0.25.

A parameter ε is introduced to quantitatively describe the transition patterns. When $0<\varepsilon<1$, the transition is abrupt, and when $\varepsilon>1$, the transition is smooth. With the increase of ε, the transition becomes smoother. Furthermore, a quantitative criterion based on the velocity ratio $\Phi = U_0/U_{CJ}$ is established to predict the transition patterns. For a given wedge angle θ, there is a critical velocity ratio Φ^*. An empirical formula between Φ^* and θ is summarized from numerical simulations, that is $\Phi^* = 0.0012\theta^2 - 0.0579\theta + 2.072$. An error limit of 2% is introduced to avoid the critical area near Φ^*. In conclusion, when $\Phi < 0.98\Phi^*$, an abrupt transition appears and when $\Phi > 1.02\Phi^*$, a smooth transition occurs.

Acknowledgements

This work is supported by National Natural Science Foundation of China (grant numbers 91441101, 51476186).

References

[1] K. Kailasanath, Review of propulsion applications of detonation waves, AIAA J. 38 (9) (2000) 1698–1708.
[2] B. Parent, J.P. Sislian, J. Schumacher, Numerical investigation of the turbulent mixing performance of a cantilevered ramp injector, AIAA J. 40 (8) (2002) 1559–1566.
[3] D.C. Alexander, J.P. Sislian, B. Parent, Hypervelocity fuel/air mixing in mixed-compression inlets of scramjets, AIAA J. 44 (10) (2006) 2145–2155.
[4] P. Wolański, Detonative propulsion, Proc. Combust. Inst. 34 (2013) 125–158.
[5] C. Li, K. Kailasanath, E.S. Oran, Stability of Oblique Detonations in Ram Accelerators, AIAA Paper, 1992.
[6] C. Li, K. Kailasanath, E.S. Oran, Detonation structures behind oblique shocks, Phys. Fluids 6 (4) (1993) 1600–1611.
[7] J.C. Broda, An Experimental Study of Oblique Detonation Waves (ph.D. thesis), Connecticut University, 1993.
[8] V.V. Vlasenko, V.A. Sabelńikov, Numerical simulation of inviscid flows with hydrogen combustion behind shock waves and in detonation waves, Combust. Explos. Shock Wave 31 (3) (1995) 376–389.
[9] C. Viguier, L.F. Figueira Da Silva, D. Desbordes, B. Deshaies, Onset of oblique detonation waves: comparison between experimental and numerical results for hydrogen-air mixtures, Symp. (Int.) Combust. Elsevier 26 (1996) 3023–3031.
[10] M.Y. Gui, B.C. Fan, Wavelet structure of wedge-induced oblique detonation waves, Combust. Sci. Technol. 184 (10–11) (2012) 1456–1470.
[11] Y. Liu, D. Wu, S.B. Yao, J.P. Wang, Analytical and numerical investigations of wedge-induced oblique detonation waves at low inflow Mach number, Combust. Sci. Technol. 187 (6) (2014) 843–856.
[12] Y. Liu, Y.S. Liu, D. Wu, J.P. Wang, Structure of an oblique detonation wave induced by a wedge, Shock Waves 26 (2) (2016) 161–168.
[13] M.H. Lefebvre, T. Fujiwara, Numerical modeling of combustion processes induced by a supersonic conical blunt body, Combust. Flame 100 (1) (1995) 85–93.
[14] M.V. Papalexandris, A numerical study of wedge-induced detonations, Combust. Flame 120 (4) (2000) 526–538.
[15] H.H. Teng, Y.N. Zhang, Z.L. Jiang, Numerical investigation on the induction zone structure of the oblique detonation waves, Comput. Fluids 95 (2014) 127–131.
[16] H.H. Teng, H.D. Ng, Z.L. Jiang, Initiation characteristics of wedge-induced oblique detonation waves in a stoichiometric hydrogen-air mixture, Proc. Combust. Inst. 36 (2) (2017) 2735–2742.
[17] L.F. Figueira Da Silva, B. Deshaies, Stabilization of an oblique detonation wave by a wedge: a parametric numerical study, Combust. Flame 121 (1) (2000) 152–166.
[18] A.F. Wang, W. Zhao, Z.L. Jiang, The criterion of the existence or inexistence of transverse shock wave at wedge supported oblique detonation wave, Acta Mech. Sin. 27 (5) (2011) 611–619.
[19] H.H. Teng, Z.L. Jiang, On the transition pattern of the oblique detonation structure, J. Fluid Mech. 713 (2012) 659–669.
[20] R. Deiterding, Parallel Adaptive Simulation of Multi-dimensional Detonation Structures, Cottbus (ph.D. thesis), Brandenburg University of Technology Cottbus, Germany, 2003.
[21] X.D. Cai, J.H. Liang, R. Deiterding, Z.Y. Lin, Detonation simulations in supersonic combustible mixtures with nonuniform species, AIAA J. (2016) 1–14.
[22] X.D. Cai, J.H. Liang, R. Deiterding, Z.Y. Lin, Adaptive simulations of cavity-based detonation in supersonic hydrogeneoxygen mixture, Int. J. Hydrogen Energy 41 (2016) 6917–6928.
[23] X.D. Cai, J.H. Liang, R. Deiterding, Y.G. Che, Z.Y. Lin, Adaptive mesh refinement based simulations of three-dimensional detonation combustion in supersonic combustible Mixtures with A Detailed reaction model, Int. J. Hydrogen Energy 41 (4) (2016) 3222–3239.
[24] X. Han, Research on Detonation Initiation and Propagation Mechanisms in Supersonic Premixed Flows, ph.D. thesis), National University of Defense Technology, Changsha, China, 2013.
[25] Z.Y. Lin, Research on Detonation Initiation and Development Mechanisms in Elevated Temperature Supersonic Premixed Mixture (Ph.D. thesis), National University of Defense Technology, Changsha, 2008.
[26] C. Li, K. Kailasanath, E.S. Oran, Effects of Boundary Layers on Oblique-detonation Structures, AIAA Paper, 1993.
[27] J. Verreault, A.J. Higgins, Formation and structure of steady oblique and conical detonation waves, AIAA J. 50 (8) (2012) 1766–1772.
[28] J.Y. Choi, I.S. Jeung, Y. Yoon, Computational fluid dynamics algorithms for unsteady shock-induced combustion, Part 1: validation, AIAA J. 38 (7) (2000) 1179–1187.
[29] D.R. Stull, H. Prophet, JANAF Thermodynamical Tables, 1971.
[30] W.Y. Crutchfield, M.L. Welcome, Object-oriented implementation of adaptive mesh refinement algorithms, Sci. Program. 2 (4) (1993) 145–156.
[31] E.F. Toro, Riemann Solvers and Numerical Methods for Fluid Dynamics, Berlin: Heidelberg, second ed., 1999.
[32] S. Browne, J. Ziegler, J.E. Shepherd, Numerical solution methods for shock and detonation jump conditions, Energy Conserv. 1 (w2) (2004) w2.